

PROCEEDINGS OF SPIE

[SPIDigitalLibrary.org/conference-proceedings-of-spie](https://spiedigitallibrary.org/conference-proceedings-of-spie)

Impact of multireflections on measurement accuracy in the endoscopic 3D reconstruction of gearing geometries

Hinz, Lennart, Kästner, Markus, Reithmeier, Eduard

Lennart Hinz, Markus Kästner, Eduard Reithmeier, "Impact of multireflections on measurement accuracy in the endoscopic 3D reconstruction of gearing geometries," Proc. SPIE 11782, Optical Measurement Systems for Industrial Inspection XII, 117821D (20 June 2021); doi: 10.1117/12.2592599

SPIE.

Event: SPIE Optical Metrology, 2021, Online Only

Impact of Multireflections on Measurement Accuracy in the Endoscopic 3D Reconstruction of Gearing Geometries

Lennart Hinz^a, Markus Kästner^a, and Eduard Reithmeier^a

^aInstitute of Measurement and Automatic Control, An der Universität 1, Garbsen, Germany

ABSTRACT

Optical triangulation systems based on fringe projection profilometry have emerged in recent years as a complement to traditional tactile devices. Due to the good scalability of the measurement approach, a highly compact novel sensor for maintenance and inspection in narrow spaces is realized by applying optical fiber bundles. Especially in the field of high-resolution and rapid maintenance in industrial environments, numerous applications arise. The endoscopic three dimensional reconstruction of gearing geometries is of particular technical relevance for detecting and quantifying damage or wear. The measurement performance depends to a considerable extent on the technical surface to be inspected. Polished surfaces are particularly problematic due to specular reflections, but can still be partially reconstructed by using HDR imaging. However, if multireflections occur in such a way that the optical path of each corresponding camera pixel can no longer be reconstructed unambiguously, a measurement is no longer feasible. In this study, the effects of surface roughness and texture, sensor arrangement, and triangulation angle on measurement error are systematically assessed to identify potential application limits and provide guidance for sensor operation.

Keywords: endoscopy, fringe projection, multireflection, specular reflection, production metrology, gear inspections

1. INTRODUCTION

Continuous developments in digital camera technology and computer-based data processing have enabled digital optical measurement devices to be found in many industrial and medical applications.¹ In the field of dimensional coordinate metrology in particular, optical measuring instruments are increasingly replacing or complement conventional, tactile sensors while opening up new application possibilities. Optical 3D scanners can reconstruct millions of surface points in a fraction of a second, thus enabling holistic evaluation and quantification of the scene and feature a compact, lightweight and cost effective design.^{2,3} For modern industrial manufacturing processes, featuring a high level of integration and automation, optical measuring technologies are an important way to ensure sufficient inline inspection capability.

Sheet-bulk metal forming (SBMF) is an innovative and novel production process which produces complex component geometries such as gears in a multi-stage, combined forming process in order to reflect current trends and challenges such as lightweight construction and resource conservation.^{4,5} For automated tool inspection, a 3D endoscope based on fiber-optic fringe projection profilometry (FPP) is automatically robot-guided into the forming plant between successive forming cycles in order to perform in-situ inspections of the tool and to metrically quantify possible wear effects during the forming process.⁶

2. PROBLEM

In contrast to tactile scanning, non-contact, optical measuring instruments are dependent on reflected light and thus on the optical properties of the specimen surface. This applies in particular to triangulation-based measuring principles, such as fringe projection profilometry, which requires unambiguous determination of the optical beam path for accurate reconstruction. Transparent or translucent object surfaces in particular therefore preclude or

Further author information: (Send correspondence to Lennart Hinz)

Lennart Hinz: E-mail: lennart.hinz@imr.uni-hannover.de, Telephone: +49 - 511 - 762 3235

Optical Measurement Systems for Industrial Inspection XII, edited by Peter Lehmann, Wolfgang Osten, Armando Albertazzi Gonçalves, Proc. of SPIE Vol. 11782, 117821D
© 2021 SPIE · CCC code: 0277-786X/21/\$21 · doi: 10.1117/12.2592599

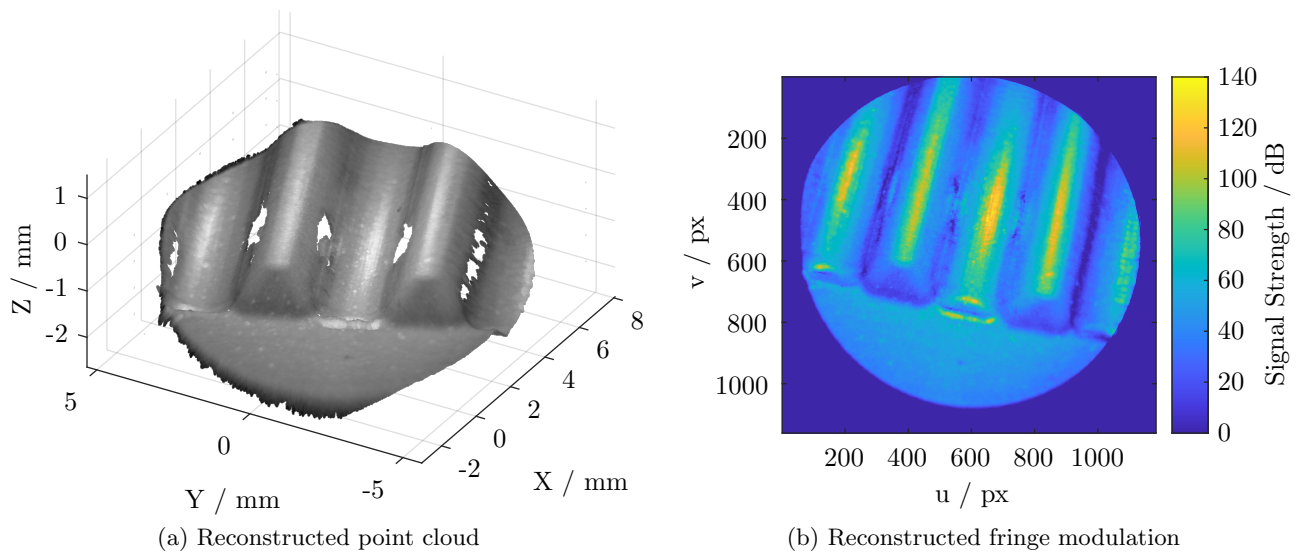


Figure 1: Application of a fiber optic endoscopic fringe projection system on a shiny gearing tool surface

restrict a possible application.⁷ In this context, lubricants can also pose a significant metrological problem, as specimen geometries often have to be inspected in an unclean condition, especially in the field of production metrology.⁸ On the other hand, specular reflecting technical surfaces can have a significant negative impact on the reconstruction result, since the camera sensor of the stereoscopic system tend to be locally overexposed by the specular reflection when positioned and oriented improperly. By combining differently exposed images, the overall dynamic range of the sensor is increased (HDR imaging) and thus also strong differences in brightness can be resolved. However, additional measurement noise is likely, which limits the reconstruction accuracy.⁷ Figure 1a shows a three-dimensional point cloud of a gearing geometry produced with SBMF. Figure 1b shows the modulation signal strength of the highest projected fringe frequency of the corresponding camera image. Shiny spots appearing on the tooth heads and tooth roots are significantly visible. However, it can be seen in the 3D data that corresponding areas were reconstructed. Nevertheless, distinct reconstruction holes appear in the area of the tooth flanks. The erroneous areas can also be found in the form of image artifacts in Figure 1b. In contrast to shadowing effects, however, in this case, especially in the area between the two central tooth flanks, the surface is completely within the viewing cones of both camera and projector. This local improper surface reconstruction is therefore more likely to be caused by the smooth technical surface in combination with the toothing geometry, which causes bouncing of the beams between the opposing tooth flanks, rendering the reconstruction of the beam path impossible. This effects, referred to as multireflections, are particularly pronounced in the reconstruction of gearing geometries, but can also be found in other measurement applications, for example in the endoscopic inspection of jet engine components.⁹ Since the phenomenon depends on the surface properties of the specimen, the object geometry and the sensor pose and orientation as well as the arrangement of the stereoscopic components, approaches for the estimation of an optimal sensor pose are very complex and require an extensive simulation environment. In the context of this study it is therefore investigated to what extent the effect can be sufficiently quantified with systematic investigations on an adjustable standard to provide a knowledge base for an optimal sensor positioning in the reconstruction of gearing geometries using a triangulating 3D endoscope.

3. EXPERIMENTAL SETUP

The experiments performed in this study are mainly based on the endoscopic fiber optic fringe projection sensor, which was developed within the scope of the Transregional Collaborative Research Center (TCRC) 73. The main components include a GS3-U3-23S6M-C CMOS industrial camera (FLIR Systems, Wilsonville, OR, United States) using the IMX174 sensor from Sony Group Corporation (Tokyo, Japan) and a DLP 7000 micromirror array from Texas Instruments Incorporated (Dallas, TX, United States). By binary tilting of the micromirrors,

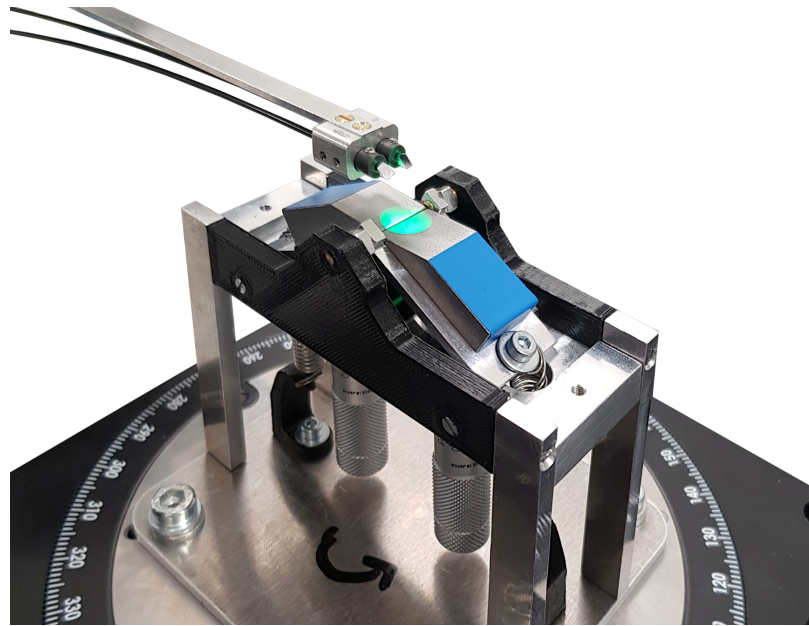


Figure 2: Experimental setup with fiber optic 3D endoscope and gear wheel standard on a rotation stage

structured light in the form of phase-encoded fringe patterns is generated and coupled via an infinity-corrected microscope objective (10 x, NA = .25) in combination with a tube lens ($f = 150\text{mm}$) into an image guide bundle of the type FIGH-100-1500N from Fujikura Ltd. (Tokyo, Japan). The fiber bundle features a length of one meter and includes 100,000 individual fiber cores and is also applied for the observation of the scene. The light source consists of a GT CSSPM (Oslo SSL) high power LED with a peak wavelength of 521 nm which is supplied by Osram Light AG (Munich, Germany) in combination with a Köhler illumination arrangement. For further information as well as the models and algorithms for system calibration and the reconstruction pipeline, reference is made to previous publications.^{6,7,10}

Figure 2 shows a picture of the main experiment of this study. The fiber optic 3D endoscope is positioned above a gear wheel standard. The tilt of the reference surfaces can be adjusted via two micrometer screws to simulate different profile angles.¹¹ To investigate the influence of the orientation of the standard to the sensor respectively of the calibrated fringe projection angle, the setup is mounted on a rotary stage of type URS 150 BCC from Newport Corporation (Irvine, CA, United States) with a guaranteed bidirectional repeatability of ± 1.1 mdeg. Figure 3 shows a detailed schematic overview of the measuring head. Two identical gradient index (GRIN) rod lenses of type GT-IFRL-200-020-50-P9 from GrinTech GmbH (Jena, Germany) with a working

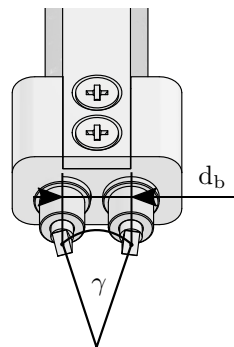


Figure 3: Schematic overview of the respective measuring head configurations

Index	d_b / mm	γ / deg
1	5.00	16.96
2	6.00	26.34
3	8.15	35.03

Table 1: Adjusted triangulation angle γ with respect to the distance of the imaging optics d_b

distance of 20 mm and an attached 90 degree mirror prism each are applied. Since it can be assumed that the illumination and observation angle is of considerable importance for this experiment and the occurring reflections, three different measuring head designs with differently configured triangulation bases are applied for this study. Table 1 specifies the spacing d_b with respect to the triangulation base. By rotating the optics, the mirror prisms are adjusted in such a way that the overlap of the camera and projector cones of view is maximized over the entire depth-of-field range. Both camera and projector are modeled using the pinhole camera model¹²⁻¹⁴ in combination with radial and tangential distortion correction.^{15,16} The actual triangulation angle γ can then be determined from the extrinsic calibration with respect to the triangulation basis as part of the system calibration.

A second experiment investigates the influence on different sample surfaces. Therefore, the specimen of the experimental setup from Figure 2 are changed. Figure 4 shows a comparison of the examined technical surfaces. The images were taken with a VR-3200 3D profilometer from Keyence Corporation (Osaka, Japan). The specimen in Figure 4a is supposed to represent a typical surface from industrial production. Specular reflective properties are favored by a slight polishing. The milling structures still present provide an additional directional bias. In Figure 4b, the specimen was additionally sandblasted before polishing. This creates a random structure and serves as a reference specimen for the studies on the variation of the triangulation angle γ . Figure 4c shows a supplementary specimen for which the final polishing after sandblasting was not performed. The resulting random and rough surface should be optically cooperative and hardly prone to multireflections.

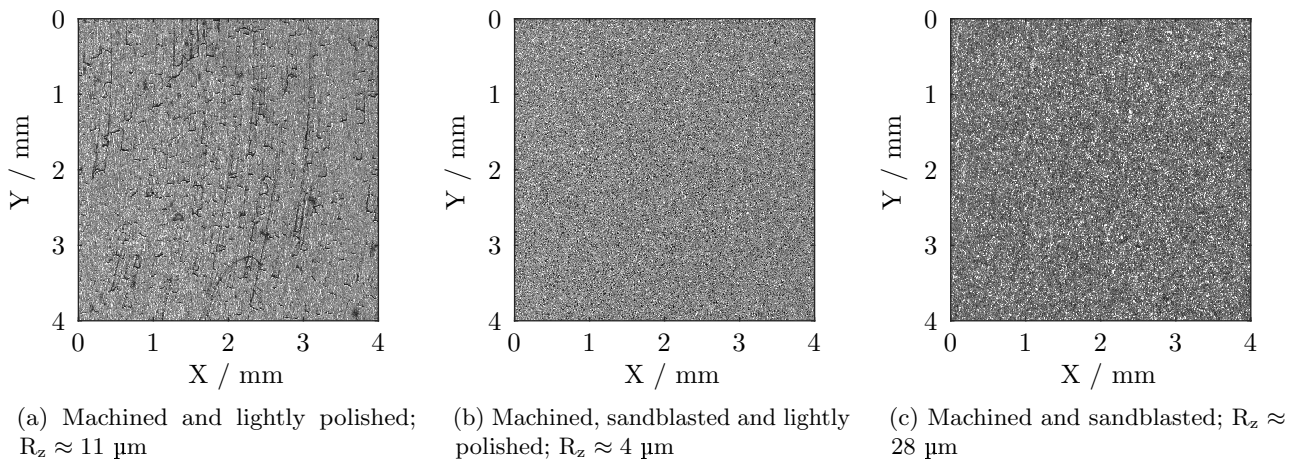


Figure 4: Comparison of the different applied technical surfaces

4. DATA PROCESSING

The reconstructed point clouds are first pre-masked using the usual data processing pipeline¹⁷ in order to remove poorly reconstructed data points or data points of insufficiently calibrated positions within the measurement volume. In the subsequent step, two planes have to be optimally fitted numerically into the data. For this purpose, 6 random points are first extracted from each measurement using a RANSAC¹⁸ approach and two planes are numerically fitted into 3 points each with 100 iterations and a random downsampling to 100,000 data points. By minimizing the sum of the absolute point deviations in normal direction $\delta_{n,abs}$, initial values for a refined plane fitting can be found. During the course of the experiments, it became apparent that this automated approach

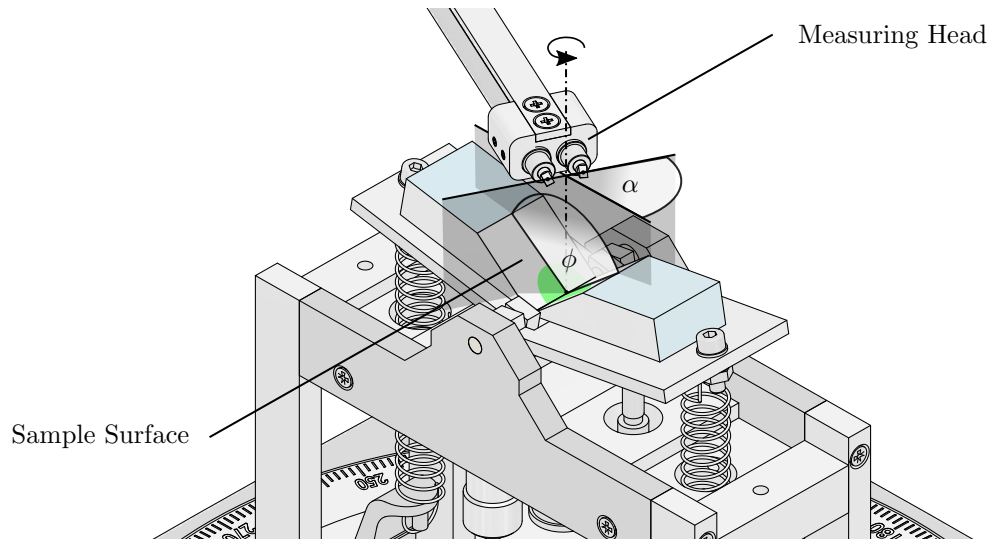


Figure 5: Geometric angular relationships on schematic overview of the experimental setup

converges more poorly the closer both planes approach parallelism and therefore does not work consistently for all data sets. As a result, only datasets with comparatively large dihedral angle ϕ , which corresponds to twice the profile angle, are initially evaluated. The transformation of the intersection line l_s of the fitted planes is estimated for each angular position α of the rotation stage with respect to the epipolar plane. An overview of the geometric relationships is given in Figure 5. The corresponding point clouds are transformed to the origin so that the line of intersection l_s is aligned with the Y axis. The rotational alignment around l_s is done via the normal directions of the two fitted planes. From these reference transformations, a hand-eye correspondence is then estimated using the position data from the forward kinematics in order to optimally align all data sets. Figure 6a shows the alignment of such a measurement. For the final deviation determination, the data are split with respect to the YZ plane and the plane fit is performed twice with an inlier interval of $\pm 2\sigma$. In the region of the plane intersection, significantly artifacts and many missing surface points are visible. To provide a quantitative assessment, the standard deviation $\sigma_{\text{diffs,all}}$ of all absolute point deviations in normal direction $\delta_{n,\text{abs}}$ is calculated. In order to evaluate the noise of all robustly reconstructed surface points belonging to each actual plane, independent of the

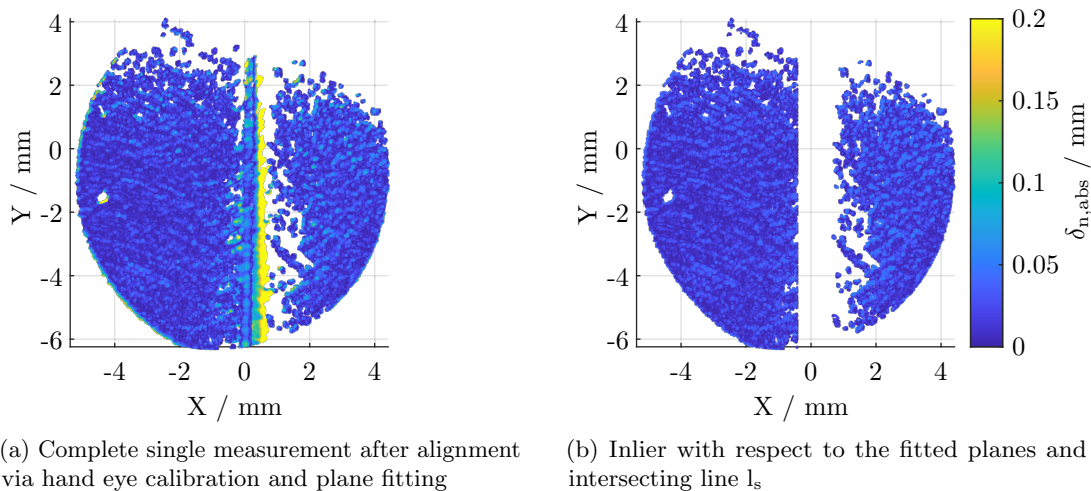


Figure 6: Aligned single measurement with significant multi-reflection artifacts and missing surface points

presence of artifacts, an additional outlier removal is carried out. Therefore all data points with $\delta_{n,abs} > 150 \mu\text{m}$ as well as a distance to the plane intersection line l_s of maximum $500 \mu\text{m}$ are trimmed and $\sigma_{\text{diffs,in}}$ is calculated accordingly. As a supplementary metric, the total number of points in the inlier dataset n_{pts} is extracted. For each data set, about 30 angular positions are adjusted with each measured at 45 positions of the rotation stage. The data generation and evaluation of each specimen takes about one day.

5. RESULTS

5.1 Variation of the triangulation angle γ

The following results, presented in Figure 7, refer to the technical surface from Figure 4b with sandblasted and polished finishing. Figures 7a to 7c show the results $\sigma_{\text{diffs,all}}$ including all triangulation artifacts. All results show a clear increase from a dihedral angle of $\phi < 135 \text{ deg}$. This seems to be especially evident for a rotation angle of $\alpha \pm 90 \text{ deg}$. According to figure 5, this represents the case where the epipolar plane approaches parallelism to the symmetry plane between the two surfaces. It is noticeable that for $\alpha \approx 0 \text{ deg}$ and $\alpha \pm 180 \text{ deg}$ there is almost no significant deviation. When comparing the different sensor configurations, it is remarkable that a larger triangulation angle γ has a significantly positive influence on the results and enables better reconstruction at smaller dihedral angles ϕ . Figures 7d to 7f show the results for the deviations without outlier and artifacts and thus represents surface noise. In accordance with the previous observations, it is noticeable that the noise increases for $\alpha \pm 90 \text{ deg}$. Overall, however, a larger dihedral angle ϕ has a negative influence on the results. The radial position α is therefore less relevant for the pure surface noise with respect to $\sigma_{\text{diffs,in}}$. It is also noticeable that a larger triangulation angle γ significantly reduces the measurement noise.

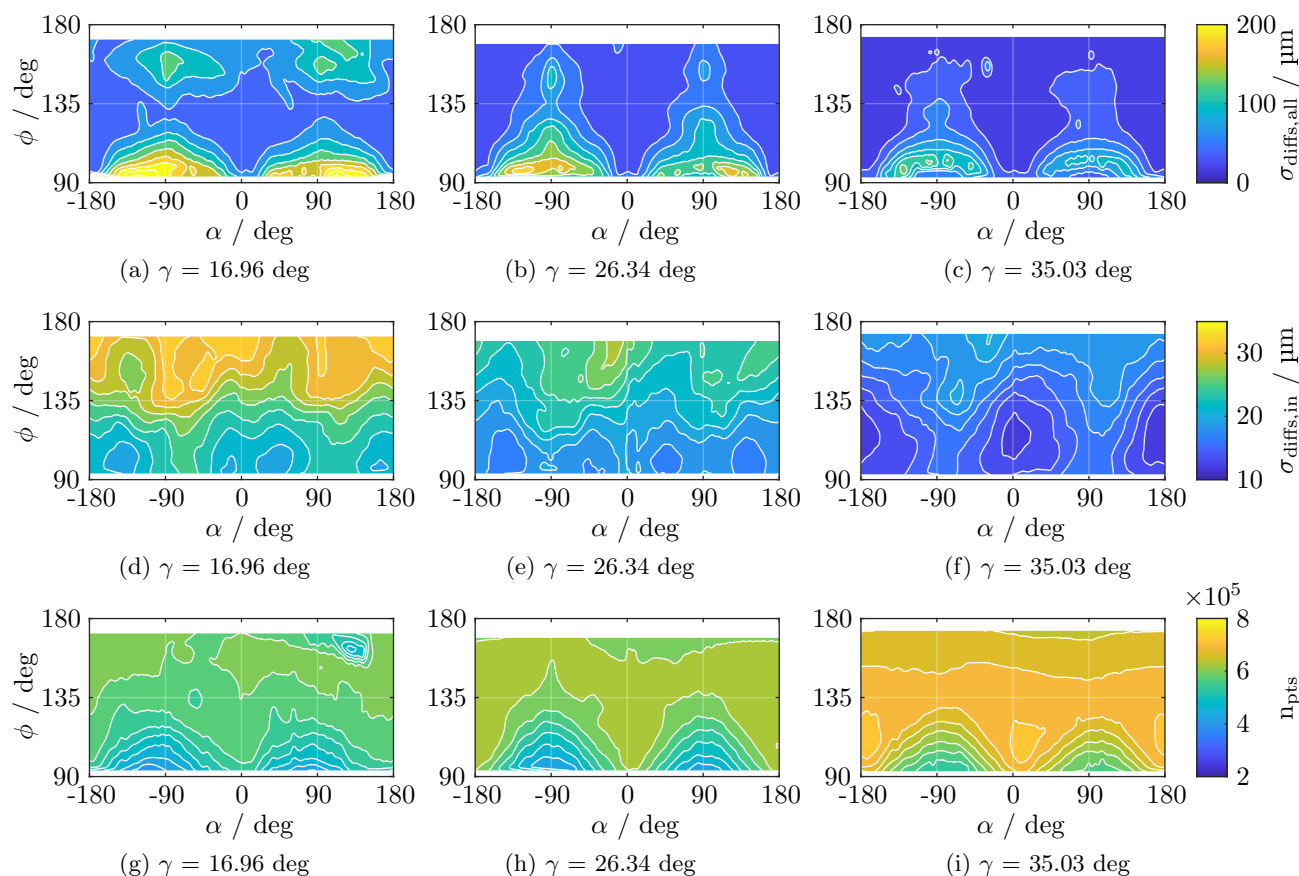


Figure 7: Effect of rotation angle α and dihedral angle ϕ on $\sigma_{\text{diffs,all}}$, $\sigma_{\text{diffs,in}}$ and n_{pts} for the technical surface from Figure 4b at different triangulation angles

Figures 7g to 7i show the results for the number of reconstructed points n_{pts} after outliers and artifacts have been removed from the data. Again, a significant negative influence at $\alpha \pm 90$ and $\phi < 135$ deg is observable. The number of reconstructed points increases with a larger triangulation angle γ . It is also noticeable, especially in Figure 7i, that the number of points n_{pts} decreases again for more obtuse dihedral angles ϕ .

5.2 Differently reflecting and textured surfaces

In the following, all technical surfaces from Figure 4 are examined at a fixed triangulation angle of $\gamma = 26.34$ deg. Thus, parts of the results were also already examined in section 5.1. Due to the strongly varying surface properties, a logarithmic scale is applied. In Figure 8 the results of the conducted experiments are presented. As previously anticipated, the sandblasted specimen according to Figures 8c, 8f and 8i shows the highest optical cooperativity and is only slightly affected by the effect of the multireflections. However, a slight influence with respect to the rotation angle α can also be observed here. Analogously, it can also be seen here that a slight surface inclination yields better results than a flat specimen.

On the other hand, the slightly polished surface with the machine processing grooves (see Figure 4a) exhibits the poorest results and, according to Figures 8a, 8d and 8g, is significantly affected by multireflections at the angular positions $\alpha \pm 90$ deg. In particular, at dihedral angles in the range of $\phi \rightarrow 90$ deg, the point cloud collapses almost completely at unfavorable rotation angles α . It is noticeable that, according to Figure 8a, the surface noise not only increases again for more obtuse dihedral angles ϕ , but also shows significant deviations for

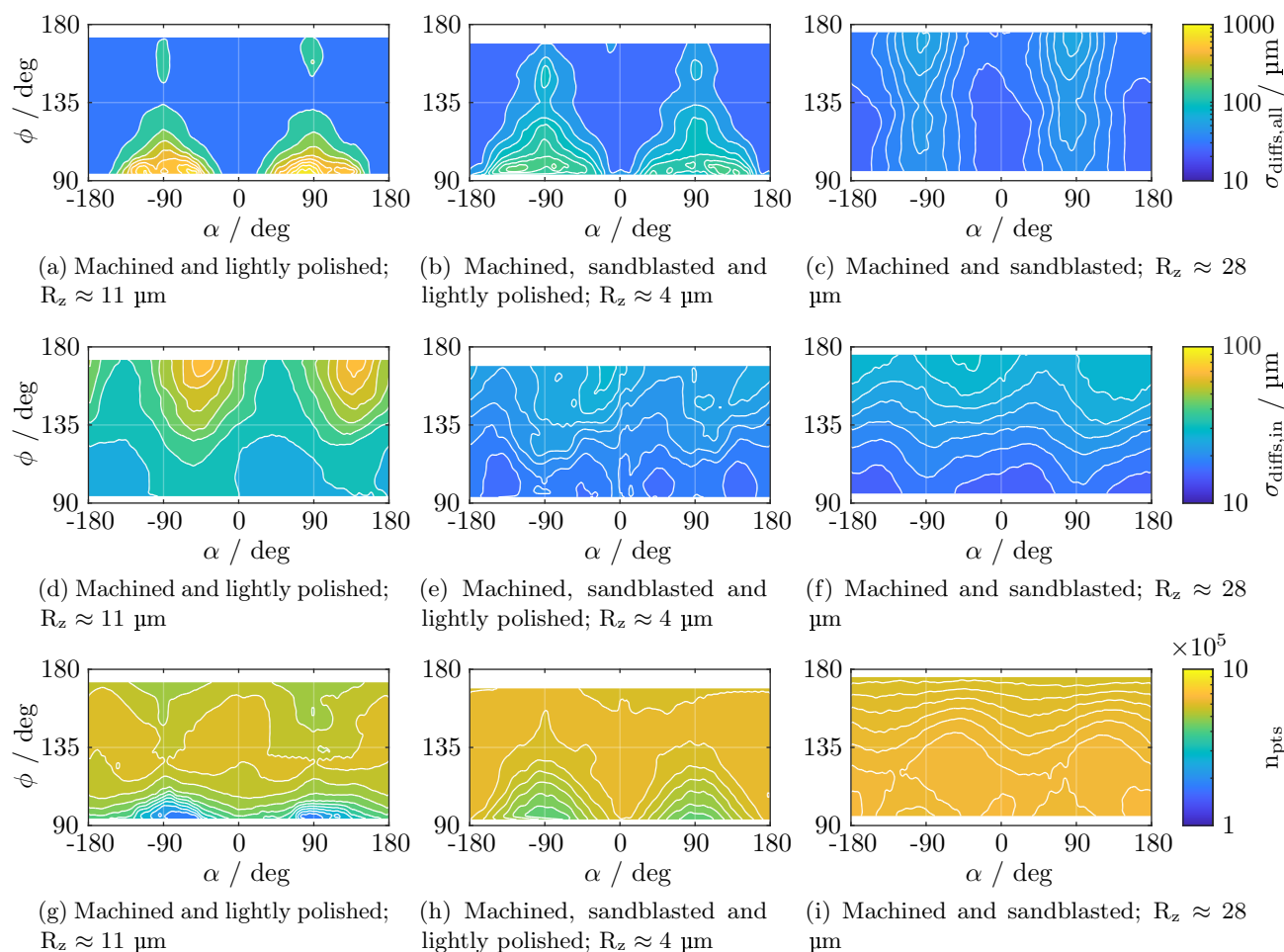


Figure 8: Effect of rotation angle α and dihedral angle ϕ on $\sigma_{diffs,all}$, $\sigma_{diffs,in}$ and n_{pts} for all technical surfaces from Figure 4 at a fixed triangulation angle of $\gamma = 26.34$ deg

$\alpha \approx -45 \text{ deg} \vee \alpha \approx 135 \text{ deg}$. This is presumably caused by the surface microstructure's direction, which results in unfavourable reflections at these angles.

6. CONCLUSION

The experiments presented in this study have shown that there is a significant influence of the profile angle or dihedral angle ϕ and orientation relative to the triangulation base α in the reconstruction of gearing geometries, especially for reflecting surfaces. With the metrics introduced, the effect of multireflection could be identified and quantified. In addition, the influence of different surface types and triangulation angles γ was investigated. Based on the results, an adequate sensor positioning is possible in order to minimize the influence of multireflections and to evaluate the feasibility of a possible inspection application depending on the sample geometry.

However, the conducted experiments also provide some additional conclusions beyond the pure multireflection phenomena. In particular, it was possible to determine and quantify the extent to which an inclined object surface reduces measurement noise and increases the total number of reconstructed data points. It can be assumed that a tilted orientation favors the imaging of diffuse-reflected light on the camera sensor, while direct, specular reflections are directed towards the camera at obtuse angles. This may also explain the extent to which additional triangulation artifacts occur even at obtuse angular positions, at which in principle the multireflection effect would no longer be expected. A dihedral angle of $\phi \approx 135 \text{ deg}$ appears to reduce the influence of multireflections, while specular reflections (without further intermediate reflections) are not yet directed towards the camera sensor.

Furthermore, the influence and the inclination effect of oriented structured surfaces could be observed. This effect is detached from multireflections on gearing geometries. Nevertheless, the results presented in this study can be helpful for sensor positioning.

With regard to the determination of the triangulation base, it could be demonstrated that an increase of the triangulation angle γ suppresses the effect of the multireflections and at the same time reduces surface noise. The latter is basically to be expected, since a larger triangulation angle γ increases the lateral displacement on the sensor and increases the vertical resolution, while reducing the measurable height range.

7. FURTHER RESEARCH

Based on this study, many follow-up investigations are conceivable. First of all, the different physical interactions reflected in the measurement data have to be distinguished from each other with additional, separate experiments. This applies in particular to the occurrence of multireflections and simple, directional specular reflections. But also the influence and the orientation of surface structures should be evaluated more closely and with supplementary experiments. Furthermore, there are many other influencing factors concerning the measurement data noise. For example, it was not taken into account in these experiments that by adjusting the dihedral angle ϕ , the overall working distance also varies. Although the sample is within the measurement range at all times, it can be assumed that there is a correlation between the working distance and the local phase measurement uncertainty and thus measurement noise within the measurement volume.¹⁹

The influence of the sample tilt should be investigated separately in a second experiment without an opposite, reflecting surface. The positive influence of certain angular positions on the reconstructed surface noise may also depend on other factors than the local surface reflection. Thus, it has to be investigated to what extent the results differ for varying fringe frequencies, since it can be assumed that there is an optimal fringe frequency for each local surface normal with respect to the meterological structural resolution.¹⁹

Finally, it can also be evaluated to what extent even smaller dihedral angles ϕ can be set by constructive changes. The determination selected in this study covers the major parts of the phenomena of multireflections, but especially in the range of $\phi \rightarrow 90 \text{ deg}$ and with the strong occurrence of multireflections, additional investigations are recommended, since in particular Figure 7c indicates that the effect of multireflection decreases again for smaller dihedral angles ϕ . In this context, the triangulation angle γ appears to be of further significance.

ACKNOWLEDGMENTS

The authors would like to thank the German Research Foundation (DFG) for funding the project B6 "Endoscopic geometry inspection" within the Collaborative Research Center (CRC) / TR 73.

REFERENCES

- [1] Tutsch, R., “Optical three-dimensional metrology with structured illumination,” *Optical Engineering* **50**, 101507 (oct 2011).
- [2] Weckenmann, A., Kraemer, P., and Hoffmann, J., “Manufacturing metrology - state of the art and prospects,” in [*Proceedings of the 9th International Symposium on Measurement and Quality*], 1–8 (2007).
- [3] Frankowski, G. and Hainich, R., “DLP-based 3d metrology by structured light or projected fringe technology for life sciences and industrial metrology,” in [*Emerging Digital Micromirror Device Based Systems and Applications*], Hornbeck, L. J. and Douglass, M. R., eds., SPIE (feb 2009).
- [4] Kleiner, M., Geiger, M., and Klaus, A., “Manufacturing of lightweight components by metal forming,” *CIRP Annals* **52**(2), 521–542 (2003).
- [5] Merklein, M., Allwood, J., Behrens, B.-A., Brosius, A., Hagenah, H., Kuzman, K., Mori, K., Tekkaya, A., and Weckenmann, A., “Bulk forming of sheet metal,” *CIRP Annals* **61**(2), 725–745 (2012).
- [6] Hinz, L., Kästner, M., and Reithmeier, E., “A 3d measuring endoscope for use in sheet-bulk metal forming: Design, algorithms, applications and results,” in [*Lecture Notes in Production Engineering*], 239–262, Springer International Publishing (nov 2020).
- [7] Hinz, L., Kästner, M., and Reithmeier, E., “Metal forming tool monitoring based on a 3d measuring endoscope using cad assisted registration,” *Sensors* **19**, 2084 (may 2019).
- [8] Metzner, S., Reuter, T., and Hausotte, T., “Evaluation on influences of thin lubricant on fringe projection measurements,” in [*Optical Technology and Measurement for Industrial Applications Conference*], Hatsuzawa, T., Tutsch, R., and Yoshizawa, T., eds., SPIE (apr 2019).
- [9] Pösch, A., Kästner, M., and Reithmeier, E., “Fringe projection measurement of highly specular objects in presence of multi-reflection,” (01 2014).
- [10] Matthias, S., “A flexible endoscopic structured light 3-d sensor: Design, models and image processing,” (2018).
- [11] [*Gear nomenclature, definitions of terms with symbols : AGMA standard*], American Gear Manufacturers Association, Alexandria, Va, revision g05 ed. (2005).
- [12] Zhang, Z., “A flexible new technique for camera calibration,” *IEEE Transactions on Pattern Analysis and Machine Intelligence* **22**(11), 1330–1334 (2000).
- [13] Bouguet, J.-Y., “Camera calibration toolbox for matlab,” (2015).
- [14] Heikkila, J. and Silven, O., “A four-step camera calibration procedure with implicit image correction,” in [*Proceedings of IEEE Computer Society Conference on Computer Vision and Pattern Recognition*], IEEE Comput. Soc (1997).
- [15] Conrady, A. E., “Decentred lens-systems,” *Monthly Notices of the Royal Astronomical Society* **79**, 384–390 (mar 1919).
- [16] Brown, D. C., “Close-range camera calibration,” *Photogrammetric Engineering* **37**(8), 855–866 (1971).
- [17] Hinz, L., Kästner, M., and Reithmeier, E., “Adaptive merging of large datasets of a 3d measuring endoscope in an industrial environment,” in [*Optics and Photonics for Advanced Dimensional Metrology*], de Groot, P. J., Leach, R. K., and Picart, P., eds., SPIE (apr 2020).
- [18] Fischler, M. A. and Bolles, R. C., “Random sample consensus,” *Communications of the ACM* **24**, 381–395 (jun 1981).
- [19] Hinz, L., Metzner, S., Müller, P., Schulte, R., Besserer, H.-B., Wackenrohr, S., Sauer, C., Kästner, M., Hausotte, T., Hübner, S., Nürnberger, F., Schleich, B., Behrens, B.-A., Wartzack, S., Merklein, M., and Reithmeier, E., “Fringe projection profilometry in production metrology: A multi-scale comparison in sheet-bulk metal forming,” *Sensors* **21**, 2389 (mar 2021).